Tutorial 8: Modern particle detectors

Dr. M Flowerdew

December 17, 2014

1 Introduction

In this tutorial, we will briefly review the techniques that are most commonly used for particle detection and energy/momentum measurements in modern high-energy physics experiments, such at those of the LEP, Tevatron and the LHC. A detector such as ATLAS (see Figure 1) consists of a large number of sub-detectors, each optimised for making a particular kind of measurement. Broadly speaking, these sub-detectors are arranged as follows:

- Tracking detectors, for measuring charged particles, closest to the interaction region.
- Calorimeters, for measuring electrons, photons and hadronic jets, surrounding the tracker.
- Muon detectors surrounding the calorimeters.

In addition to this, certain experiments will have specialised sub-detectors for other purposes, for example measuring the integrated luminosity, or performing detailed particle identification such as $\pi^{\pm}/K^{\pm}$ separation. These involve many extensions of the techniques described here, for example to simultaneously measure a particle's momentum and speed to obtain its mass, often by making use of other particle/material interactions, such as Čerenkov radiation.

2 Tracking detectors

The purpose of a tracking detector, whether it is close to the interaction region or part of a muon detector, is to measure the momenta of charged particles as precisely as possible, with minimal disturbance to their flight. They are almost invariably located within a magnetic field, so that the radius of curvature of the particles within the field can be measured. This, coupled with knowledge of the particle's direction of motion in 3D space, can be used to measure its momentum.

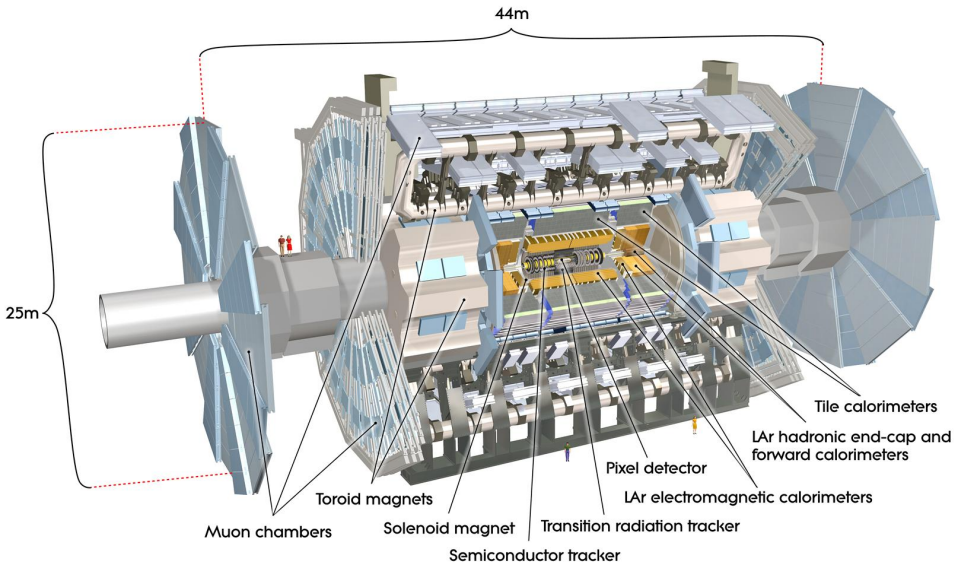

Figure 1: Cut-away view of the ATLAS detector.

Most often, the presence of a charged particle is detected by the ionisation it causes when passing through matter. This energy loss is desecribed by the Bethe-Bloch equation for a particle of charge q and speed βc:

$$\frac{\mathrm{d}E}{\mathrm{d}x} = -0.31\frac{Z}{A}\rho\frac{q^2}{\beta^2}\left[\ln\left(\frac{2m_e c^2\beta^2\gamma^2}{I}\right) - \beta^2 - \frac{\delta}{2}\right] \text{ MeV cm}^{-1}, \qquad (1)$$

where Z and A are the atomic and mass numbers of the material, respectively, ρ is its density, I the ionisation potential (typically about $10Z$ if Z is large) and δ is a dielectric screening correction that is important when $\gamma >> 1$.

The energy loss from ionisation and other sources for a muon passing through copper is shown as a cfunction of $\beta\gamma$ in Figure 2. Although the details, including the magnitude of the energy loss, depend on the particle and material, the qualitative features of the curve as a function of $\beta\gamma$ are similar for most particles and most materials. There is a large region in particular, for $1 \lesssim \beta\gamma \lesssim 1000$, where the energy loss is small - for muons in copper this corresponds to momenta of around 0.1–100 GeV. Particles in this "minimum ionising" range will liberate enough electric charge to be detected, but will not be stopped by the material. Still, it is desirable to extract the greatest number of measurement points ("hits") with the minimum possible amount of material. This is in order to reduce the effects of multiple scattering, which we will return to later.

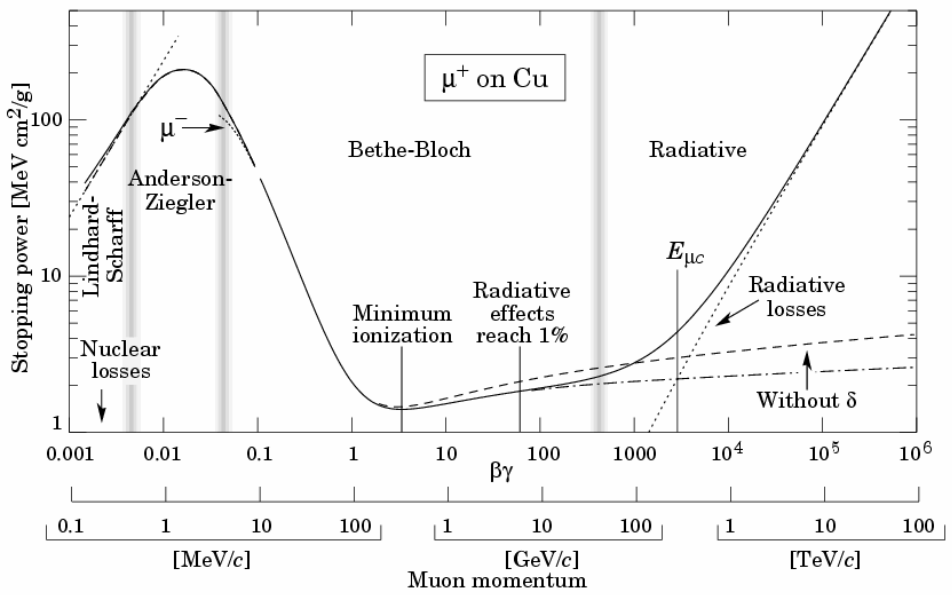

Figure 2: Illustration of the energy loss of muons in copper, as a function of $\beta\gamma$ of the muon and its momentum.

2.1 Drift tube detectors

Many tracking detectors are made from arrays of *drift tubes*, such as the one illustrated in Figure 3. The wire located in the centre of the tube is held at a positive voltage relative to the tube wall, so that electrons liberated through ionisation will drift towards it with an average speed proportional to the local electric field, while ions migrate (more slowly) towards the wall. The electric field strength at a radius of r is proportional to $1/r$, increasing rapidly close to the wire. This allows the tube to exhibit several behaviours, depending on the wire radius a and the applied voltage V, illustrated in

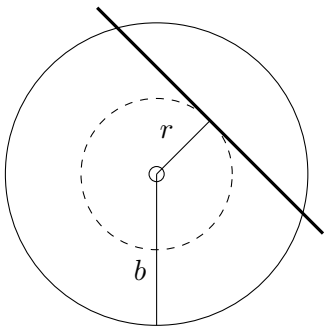

Figure 3: Cross-section of a drift tube, where a charged particle is passing through with an impact parameter of r.

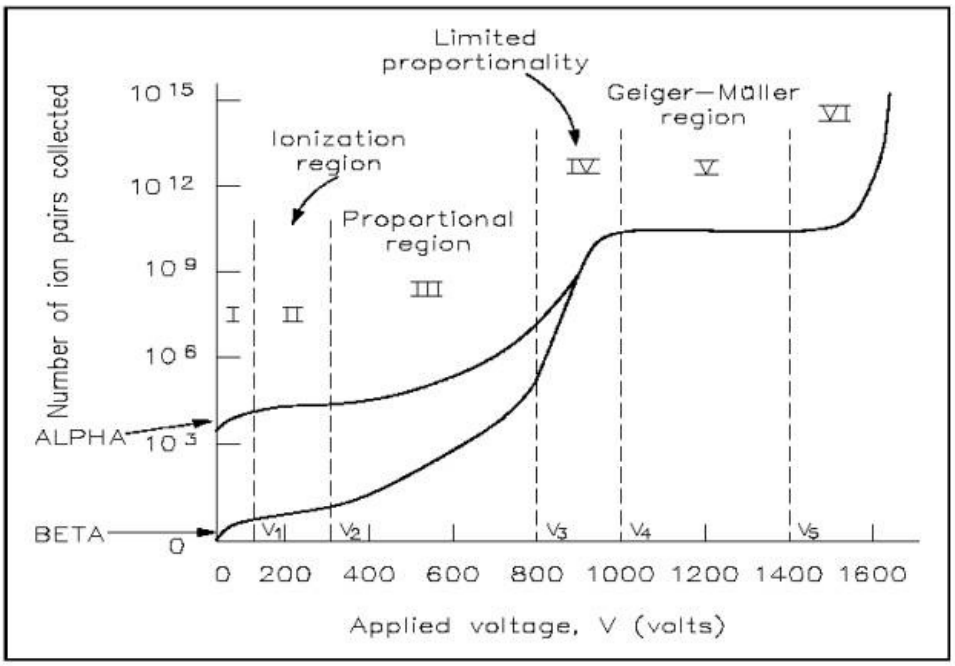

Figure 4: Response of a drift tube as a function of the applied voltage.

Figure 4. For low voltages (and large a), the ionisation electrons simply travel to the wire, and the measured response[1] is low and constant. When the voltage is increased, the electron energy near the wire is greater than the ionisation potential, and therefore secondary ionisation occurs, leading to an *avalanche*. Initially, the response is nearly proportional to the applied voltage, but when the Geiger-Müller region is reached, saturation occurs. Drift tubes for use in tracking detectors are generally operated within the proportional regime.

Once the pulse has finished, *recombination* occurs and the tube becomes ready to accept a new signal. This process may, however, emit UV photons, which can themselves cause ionisation and another cascade. For this reason, a *quencher* is usually introduced, usually polyatomic molecules such as CO_2, hydrocarbons or alcohols, that can absorb UV photons without being ionised.

Question: How might a quencher molecule absorb a photon without being ionised or immediately re-radiating it?

The choice of gas in a drift tube is dictated by a number of factors. Noble gases have few non-ionising modes for energy loss, and therefore support avalanches at low applied voltages. Many (e.g. Ar, Xe, Kr) are massive and

[1]Depending on the individual detector, either current or voltage may be measured at the wire. Here, we will use the words "signal" and "response" to refer to either of these.

thus yield many ion/electron pairs per unit path length (called *specific ionisation*). However, argon emits 11.6 eV photons during recombination, which can lead to permanent discharge unless appropriately quenched. Polyatomic gases, by contrast, can be self-quenching if the gas is circulated, but inelastic collisions can lead to the formation of free radicals that can damage the detector.

The measurement of a signal in a drift tube does not indicate an absolute position. By precisely measuring the time at which the signal first passes some predefined threshold (time resolution: typically ∼few ns), the radius of closest approach r can be deduced, if the bunch-crossing time is known. For very precise measurements, the propagation time of the signal through the wire must also be known, which depends on how far the particle's path is from the read-out end of the tube. This is usually obtained using complementary measurements of the particle's trajectory made by another nearby sub-detector. With drift velocities typically of around 50 mm μs^{-1}, spatial resolutions of the order of $\delta r \sim 100$ μm can be achieved. To resolve ambiguities in the path of the track, measurements from many tubes must be combined - the true particle track should pass tangentially to each measured drift circle, within the precision of the measurements.

In ATLAS, very narrow drift tubes ("straws") are used in the transition radiation tracker, and 14 mm diameter drift tubes are used in the muon detector.

2.2 Silicon detectors

While relatively cheap and easy to make, drift tubes do not have sufficient resolution to distinguish hits from different particles very close to a collider's interaction region. In this region, semiconductor detectors are used, usually made using silicon. A cross-section of a silicon "strip" detector is shown in Figure 5. The sensor is essentially a collection of reverse-biased diodes. In undoped silicon at room temperature and pressure, electrons in the conduction band and holes in the valence band result in $\mathcal{O}(10^{10})$ charge carries per cubic centimetre. This is to be compared with about 100 pairs liberated per μm path length by a minimum ionising particle. Constructing a diode by combining p- and n-doped silicon creates a depletion zone at the join, with no free carriers. Applying a reverse-baised voltage causes the entire volume to be depleted, while simultaneously producing an electric field within the sensor, allowing efficient charge collection from ionisation. Cooling the detector, for example with liquid nitrogen, also reduces the charge carrier density and the resulting leakage current. With modules typically a few hundred micrometres thick, many thousand electron/hole pairs can be formed, creating a clear signal even without further amplification.

In ATLAS, an extensive semiconductor tracker operating along these lines is used to reconstruct charged particle trajectories with a resolution

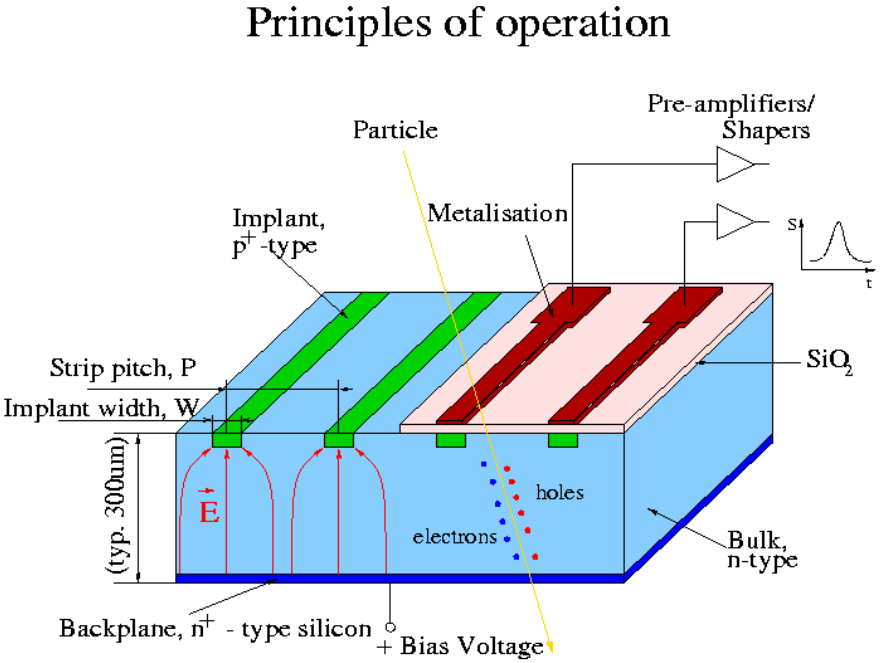

Figure 5: Schematic diagram of a p-in-n silicon strip detector. In a typical detector, the strip pitch would be of the order of μm, and the sensor thickness would be a few hundred μm. Individual strips can be several cm long.

of $\sim$ 17 μm in the direction perpendicular to the strips. Modules are arranged in back-to-back pairs, with strips aligned with a small angle (40 μm) between them, to allow measurement of the hit position along the strip. The measurement in this direction is relatively coarse, with a resolution of $\sim$ 580 μm. The modules are aligned with respect to the magnetic field to give the best possible momentum resolution.

Question: In an environment with high charged particle densities, what problems might there be if the strips on neighbouring modules were aligned at right angles to each other?

At radii of less than 250 mm, an even more precise tracking technology is used. Still based on silicon, a *pixel* detector has full two-dimensional granularity on a single chip, with pixel elements of dimension 50 μm$\times$400 μm. These give improved hit resolution of about 10 μm$\times$100 μm. Using pixels, rather than strips, not only improves the spatial resolution with less material (as back-to-back modules are not necessary), but they are also intrinsically more radiation-tolerant, suffer from lower noise levels and have fewer hit ambiguities. They are, however, significantly more complex and expensive to make.

All silicon detectors degrade over time. Radiation damage can lead to vacancies and other lattice defects that decrease the charge carrier mobility and create new interstitial energy levels within the band gap. These interstitial levels allow charge carriers through the otherwise depleted material, increasing the leakage current. Over time, type-inversion can also occur, meaning that the n-type bulk becomes more like p-type silicon. This effect can be temporarily offset by increasing the applied bias voltage, at the cost of greater leakage currents (and therefore increased power consumption). The bias voltage cannot be increased indefinitely however, as eventually the risk of discharge (i.e. sparking) will become too great.

2.3 Momentum resolution

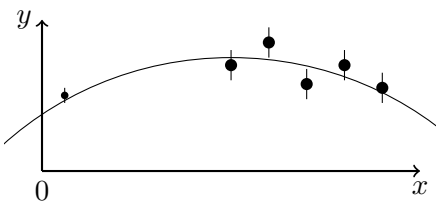

Figure 6: Sketch of a curved path fit, with contributions from one precision detector at $x \sim 0$ and five other measurements at higher x.

Figure 6 shows a sketch of a set of two-dimensional tracking detector measurements of a charged particle moving within a magnetic field B. In the absence of scattering effects (see later), the particle follows a circular path. The radius of curvature of the particle, if its momentum[2] in the $x-y$ plane is p_{T}, is

$$r = \frac{p_{\mathrm{T}}}{qB}. \tag{2}$$

The radius of curvature can be estimated by measuring the sagitta of the curve, in this case the difference in y between the highest and lowest points of the curve. Suppose that, while traversing the detector, the particle changes angle by a small amount $\phi \approx L/r$. In this case, the sagitta s can be expressed as follows:

$$\begin{aligned} s &= r - r\cos\frac{\phi}{2} \\ &\approx \frac{r\phi^2}{8} \approx \frac{qBL^2}{8p_{\mathrm{T}}}. \end{aligned} \tag{3}$$

The resolution with which s can be determined, σ_s, depends on the number of $x-y$ measurements and their intrinsic resolution. If the y measurements

[2]Here p_{T} is used, referring to transverse momentum, as the momentum in the z direction is not directly measured.

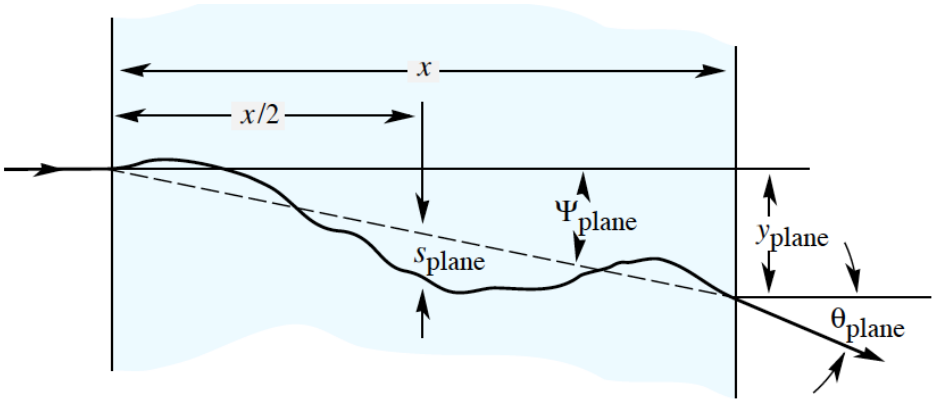

Figure 7: Illustration of multiple scattering of a particle (incident from the left) in material.

all have the same resolution σ_y, then σ_s will be proportinal to σ_y, with a constant of proportionality depending on the geometry of the detector. As s is proportional to $1/p_{\mathrm{T}}$, we can then work out how the momentum resolution $\sigma_{p_{\mathrm{T}}}$ depends on the principal parameters:

$$\frac{\sigma_{p_{\mathrm{T}}}}{p_{\mathrm{T}}} = \frac{\sigma_s}{s} \propto \frac{\sigma_y p_{\mathrm{T}}}{BL^2}. \tag{4}$$

This suggests the following design principles to obtain precise momentum measurements for particles with large p_{T}:

- a strong magnetic field B;
- a physically large detector (large L);
- good intrinsic detector resolution σ_y;
- many detector layers (not shown in Equation (4)).

The other main factor affecting the momentum resolution of a tracking detector is so-called *multiple scattering*. This, illustrated in Figure 7, describes the changes in position and direction (also energy loss) that a charged particle undergoes as it traverses material. Upon passing a distance x through a material, a particle will emerge with a displacement y_{plane} and angle θ_{plane} relative to its original trajectory.[3] In the absence of large-angle scattering, these can be described by Gaussian probability distributions with the following width parameters:

$$\theta_{\mathrm{plane}}^{\mathrm{rms}} = \theta_0 \text{ and } y_{\mathrm{plane}}^{\mathrm{rms}} = \frac{1}{\sqrt{3}} x\theta_0,$$

[3]In both cases, "plane" indicates that we are using a 2D projection. When the RMS deviations are considered, the corresponding values in 3D space are a factor of $\sqrt{2}$ larger than those quoted.

$$\text{where } \theta_0 = \frac{13.6 \text{ MeV}}{\beta cp}\sqrt{\frac{x}{X_0}}\left[1 + 0.038 \ln\left(\frac{x}{X_0}\right)\right]. \tag{5}$$

Here, X_0 is the *radiation length*, a property of the material which will be further described in the section on calorimetery (see especially Equation (8)), and a unit charge for the incident particle is assumed. Multiple scattering represents a fundamental limit on the position and angular resolution of a given detector. Recalling that the bending angle in the magnetic field, ϕ, is given by $L/r = qBL/p_{\mathrm{T}}$, we can deduce the dependence of this contribution to the resolution as a function of p_{T}:

$$\frac{\sigma_{p_{\mathrm{T}}}}{p_{\mathrm{T}}} = \frac{\sigma_\phi}{\phi} \propto \frac{p_{\mathrm{T}}}{BL}\frac{\sqrt{L}}{p_{\mathrm{T}}} = \frac{1}{B\sqrt{L}}, \tag{6}$$

if we neglect the $\ln(x/X_0)$ term from Equation (5).

Exercise: Consider a muon passing through 1m of magnetised iron ($B =$ 2 T, $X_0 = 1.8$ cm). If the muon's direction of travel is measured before and after it traverses the iron, what is the best p_{T} resolution that can be expected, based on multiple scattering effects alone?

Combining Equations 4 and 6, we can write the total p_{T} resolution in the following way:

$$\frac{\sigma_{p_{\mathrm{T}}}}{p_{\mathrm{T}}} = Ap_{\mathrm{T}} \oplus B. \tag{7}$$

The first term arises from the intrinsic measurement resolution of the detector elements, while the second arises from multiple scattering, and the $\oplus$ indicates that the terms should be added in quadrature. As the form of Equation (7) suggests, multiple scattering is usually most important when p_{T} is small.

3 Calorimetry

The purpose of a calorimeter is to measure the energy of incoming particles by completely absorbing them. Coupled with a measurement of the direction of motion, this allows the 3D momentum of relativistic particles to be reconstructed. In contrast with tracking detectors, calorimeters can detect both charged and neutral particles, through a number of different processes, depending on the particle. Modern high-energy experiments take advantage of this, with separate sub-detectors optimised for electromagnetic and hadronic interactions.

3.1 Electromagnetic calorimetry

In Figure 2, it can be seen that extremely relativistic particles[4] ($\beta\gamma \gtrsim 1000$) lose energy mainly through radiation. For currently accessible energies, this is only relevant for the electron[5], given its small mass. The critical energy, E_c, for electrons, where radiative losses are greater than ionisation losses, is approximately 0.6 GeV/Z, where Z is the atomic number of the material.

The radiation of a photon by an electron in a material is illustrated in Figure 8 (a). The electron can interact coherently with an entire nucleus, giving a contribution $Z\sqrt{\alpha}$ to the amplitude. The cross section for this process is therefore proportional to $Z^2\alpha^3$. The electron can also scatter from atomic electrons, but as this is not coherent the contribution is much smaller, proportional to $Z\alpha^3$. The electron loses energy exponentially, with a rate parameterised by the *radiation length* X_0:

$$\frac{\mathrm{d}E}{\mathrm{d}x} = -\frac{E}{X_0},$$

$$\text{where } \frac{1}{X_0\,[\mathrm{cm}]} \approx 4\left(\frac{\hbar}{mc}\right)^2 Z(Z+1)\alpha^3 n_A \ln\left(\frac{184}{Z^{1/3}}\right). \tag{8}$$

Here, n_A is the number density in cm^{-3}. Note that X_0 is often quoted in g·cm^{-2}, which is related to this definition by the density ρ. The radiation length depends strongly on the material involved, decreasing rapidly for denser elements. Radiation lengths for some elementary materials follow, at a temperature of 20°C and 1 atm pressure:

Element	X_0 [cm]
air	30,400
graphite	18.8
Al	8.9
Fe	1.8
Pb	0.6

High energy photons interact with matter in a similar way to electrons, creating electron-positron pairs (see Figure 8 (b)). This is related to the diagram in Figure 8 (a) by an exchange of ingoing and outgoing particles. The cross section is therefore similar, and the characteristic length for this process is $\frac{9}{7}X_0$.

Combining these two processes allows us to build up a simple picture of what happens when a high-energy electron (or, with minor modifications, a photon) enters a dense material. After a distance $\mathcal{O}(X_0)$, it will undergo

[4]Recall that, while Figure 2 refers specifically to muons, the qualitative features are valid for all particles, if only EM interactions are considered.

[5]and, of course, the positron.

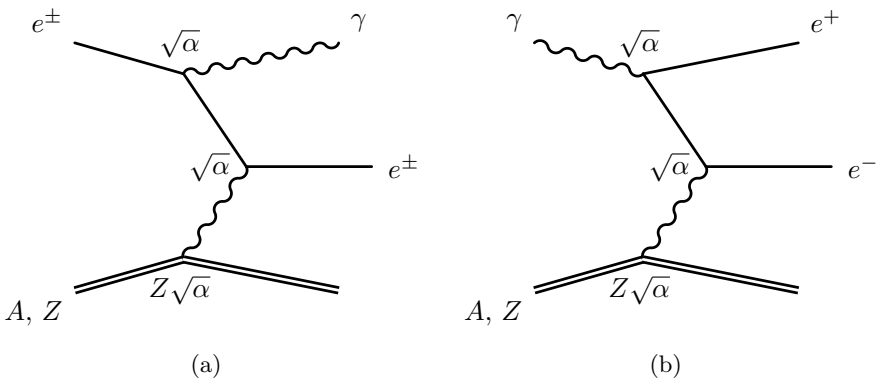

Figure 8: Diagrams for (a) Bremsstrahlung and (b) photon conversions in matter.

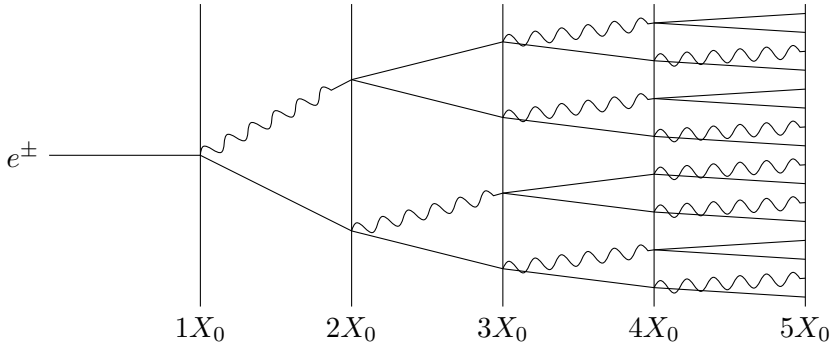

Figure 9: The Rossi model of an electromagnetic calorimeter shower.

Bremsstrahlung, producing a high-energy photon. The electron (after interaction) and the photon can be expected to have comparable energies. They will both propagate more or less freely for a further distance $\mathcal{O}(X_0)$, with the electron only losing a small fraction of its energy to ionisation of the material. Then, the electron will undergo Bremsstrahlung again, and the photon will convert into an e^+e^- pair. Again, it is reasonable to assume that all four particles (two electrons, one positron and one photon) will have comparable energies, and they will each travel a distance $\sim X_0$ before undergoing further significant interactions. This process will continue until the particles have energies below the critical energy for Bremsstrahlung, at which point all of the charged particles will lose their remaining energy through ionisation. This simple model of an *electromagnetic (EM) shower* is illustrated in Figure 9.

This model is highly simplified, and yet it illustrates certain key features of EM showers very well. Consider the shower at the n^{th} step, i.e. at a distance of nX_0 into the material. At this step, there will be 2^n particles

in the shower, each with an energy of $E_n = E_0/2^n$ (if the original incident particle had an energy E_0). The shower ends at some step N when E_N equals the critical energy E_c. Solving for N gives

$$N = \frac{\ln(E_0/E_c)}{\ln 2}. \tag{9}$$

As each step requires a distance X_0, this means that the total shower depth increases logarithmically with E_0. Although we will not prove it, the shower width is also proportional to X_0; for a shower of depth $20X_0$, the width is given approximately by $(21.2\ \text{MeV}/E_c)X_0$.

The total number of particles inside the shower is the sum of the number of particles at each step:

$$N_{\text{total}} = \sum_{n=0}^{N} 2^n = 2^{N+1} - 1 \approx 2\frac{E_0}{E_c}, \tag{10}$$

where the final equality is true if N is large. N_{total} is proportional to E_0, therefore, to measure the original particle's energy, it is sufficient just to count the number of particles in the shower! In addition, the charged particle fraction asymptotically approaches 2/3 as N grows, so it is enough just to count the number of charged particles produced.

Lead tungstate ($PbWO_4$) is a common EM calorimeter material. It has a high density and constituent atoms with high atomic numbers, and therefore a short radiation length of just 0.89 cm. In addition, it scintillates and is itself transparent to the light produced, allowing this to be collected by a photodiode or similar photodetector. However, it is brittle and can be difficult to work with. Another approach is to separate the tasks of producing and detecting the shower, by interleaving layers of a dense *absorber* (such as lead or steel) with ionisation or scintillation detectors. This design is referred to as a *sampling calorimeter*, because the shower is sampled at intervals as it evolves. The EM calorimeter in ATLAS uses this latter approach, with liquid argon (LAr) being used as the ionisation medium, while CMS has an EM calorimeter based on lead tungstate.

The proportionality between the energy and the number of shower particles is, of course, only true on average. If a particle of energy E would produce ν charged particles on average, the number observed in any particular shower will be described by Poisson statistics:

$$P(n_{\text{obs}}) = e^{-\nu}\frac{\nu^{n_{\text{obs}}}}{n_{\text{obs}}!}. \tag{11}$$

This distribution has the property that both the mean and the variance of n_{obs} are equal to ν. Variations in the energy measured will vary as $\delta(n_{\text{obs}}) = \sqrt{\text{var}(x)} = \sqrt{\nu}$. As ν is proportional to the particle's energy, the statistical

uncertainty on the energy measured will vary as $\sqrt{E}$. Equivalently, the fractional resolution σ_E/E varies as $1/\sqrt{E}$, improving as E increases.

The total energy resolution for most calorimeters can be written in the following way:

$$\frac{\sigma_E}{E} = \frac{A}{\sqrt{E}} \oplus B \oplus \frac{C}{E}. \tag{12}$$

The first term is the stochastic term just discussed. The second, constant, term arises from inhomogeneities in the calorimeter response and its calibration. The final term arises from electronic noise, and can be important for low energy particles. For the ATLAS EM calorimeter, $A = 10\%$ if E is in GeV, and $B = 0.7\%$. As before, these numbers are added in quadrature to obtain the total resolution function.

3.2 Hadronic calorimetry

Due to their higher mass[6], high-energy hadrons do not lose significant amounts of energy through electromagnetic processes (see again Figure 2). Their hadronic interactions consist of three components:

- elastic scattering from nuclei;
- quasi-elastic scattering, i.e. elastic scattering from nucleons;
- inelastic scattering.

The last two of these are responsible for producing a *hadronic shower*, with each inelastic scatter producing more hadrons that may each then undergo an inelastic collision, and so on. As with an EM calorimeter, measuring the energy of the original hadron then reduces to counting the total number of particles produced via this process.

The hadron-nucleus inelastic cross section scales with the nuclear cross-sectional area:

$$\sigma_{\text{inel}} \approx \sigma_{pp} A^{\frac{2}{3}}. \tag{13}$$

The proton-proton cross section σ_{pp} is about 30 mb, much smaller than for EM interactions. Therefore, the so-called *interaction length* λ is much longer than the EM equivalent X_0. The interaction length is defined as

$$\lambda = \frac{1}{n\sigma_{\text{inel}}}. \tag{14}$$

Typical values for some materials, which may be compared with the values for X_0 shown previously, are:

[6]The lightest hadron, the pion, has a mass similar to that of the muon.

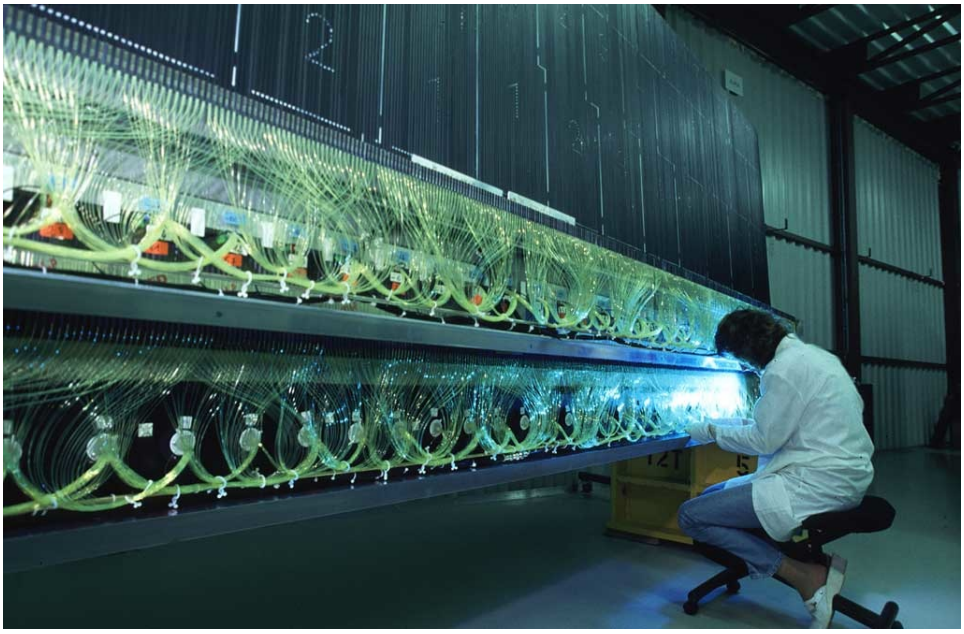

Figure 10: Part of the ATLAS hadronic calorimeter during construction.

Element	λ [cm]
air	75,000
graphite	38.1
Al	39.4
Fe	16.8
Pb	17.1

Thus, even a calorimeter made out of lead or steel will need to be very large in order to guarantee the capture of an entire hadronic shower - typically a depth of 20λ would be required. Due to the resulting size requirements, most hadronic calorimeters are of the sampling variety, with very dense, high-A absorbers. Scintillators are often used to measure the shower, where several scintillating sheets can be connected to a single photomultiplier tube via optical fibres. Such an arrangement can be seen in Figure 10. Other possibilities include collecting charge on electrode plates on either side of an ionising medium, or inserting small multi-wire proportional chambers (MWPCs) between the absorber layers.

The resolution of a hadronic calorimeter is also described by Equation (12), however the absolute values of the coefficients are usually much larger than for EM calorimeters. This is due partly to the large interaction lengths involved and the greater probability of lateral or longitudinal shower leakage, but also due to the energy lost in elastic scattering, which does not increase the number of particles in the shower. In the ATLAS hadronic calorimeter, $A = 50\%$ and $B = 3\%$.

One other factor affecting the hadronic energy resolution is that there may be EM showers contained within the hadronic shower, for example from $\pi^0 \to \gamma\gamma$ decays. The response of most calorimeters to these EM components is substantially different to the hadronic component, and the EM energy fraction is a significant source of uncertainty in the energy measurement. Usually, the response to EM showers is greater, due to the nuclear binding energy in hadronic interactions, losses from neutrinos in hadron decays, and other effects. It is possible to tune the calorimeter design to offset these effects, for example by:

- increasing the absorber thickness (which suppresses detection of EM showers);
- using a radioactive absorber, which can undergo fission in the presence of slow neutrons, increasing the overall response to hadrons;
- using light nuclei in the absorber, which can also give sensitivity to slow neutrons.

This kind of design is called a *compensating calorimeter*. A recent example of this kind of design is the ZEUS calorimeter, which used depleted uranium to increase the hadronic response. Its stochastic resolution term was indeed good, at $A = 35\%$ (compared with 50% for ATLAS). This comes with a cost however, which is the reduced response to EM showers; ZEUS' stochastic term coefficient for these was 18%, compared to 10% for ATLAS. However, precise measurements of jets for the measurement of parton density functions was a key aspect of the design of ZEUS, explaining why this trade-off was made.